Mapping the Interaction of Cofilin with Subdomain 2 on Actin†

Sabrina A. Benchaar,‡ Yongming Xie,‡ Martin Phillips,‡ Rachel R. Ogorzalek Loo,§,$ Vitold E. Galkin,◊ Albina Orlova,◊ Mario Thevis,‡,# Andras Muhlrad,|| Steven C. Almo,⊥ Joseph A. Loo,‡,§,$ Edward H. Egelman,◊ Emil Reisler*,‡,$

Department of Chemistry and Biochemistry, Molecular Biology Institute and Department of Biological Chemistry, University of California, Los Angeles, California 90095, Department of Biochemistry, Albert Einstein College of Medicine, Bronx, New York 10461, Department of Oral Biology, Hebrew University-Hadassah School of Dental Medicine, Jerusalem, Israel 91120, and Department of Biochemistry and Molecular Genetics, University of Virginia Health Sciences Center, Charlottesville, Virginia 22908

Received May 30, 2006; Revised Manuscript Received October 19, 2006

ABSTRACT: Cofilin, a member of the actin-depolymerizing factor (ADF)/cofilin family of proteins, is a key regulator of actin dynamics. Cofilin binds to monomer (G-) and filamentous (F-) actin, severs the filaments, and increases their turnover rate. Electron microscopy studies suggested cofilin interactions with subdomains 2 and 1/3 on adjacent actin protomers in F-actin. To probe for the presence of a cryptic cofilin binding site in subdomain 2 in G-actin, we used transglutaminase-mediated cross-linking, which targets Gln^{41} in subdomain 2. The cross-linking proceeded with up to 85% efficiency with skeletal α-actin and WT yeast actin, yielding a single product corresponding to a 1:1 actin−cofilin complex but was strongly inhibited in Q41C yeast actin (in which Q41 was substituted with cysteine). LC−MS/MS analysis of the proteolytic fragments of this complex mapped the cross-linking to Gln^{41} on actin and Gly^{1} on recombinant yeast cofilin. The actin−cofilin (AC) heterodimer was purified on FPLC for analytical ultracentrifugation and electron microscopy analysis. Sedimentation equilibrium and velocity runs revealed oligomers of AC in G-actin buffer. In the presence of excess cofilin, the covalent AC heterodimer bound a second cofilin, forming a 2:1 cofilin/actin complex, as revealed by sedimentation results. Under polymerizing conditions the cross-linked AC formed mostly short filaments, which according to image reconstruction were similar to uncross-linked actin−cofilin filaments. Although a majority of the cross-linking occurs at Gln^{41}, a small fraction of the AC cross-linked complex forms in the Q41C yeast actin mutant. This secondary cross-linking site was sequenced by MALDI−MS/MS as linking Gln^{360} in actin to Lys^{98} on cofilin. Overall, these results demonstrate that the region around Gln^{41} (subdomain 2) is involved in a weak binding of cofilin to G-actin.

The (ADF)/cofilin[1] family of proteins is involved in regulation of actin dynamics, affecting many aspects of cell physiology, including cell division (*1*, *2*), cell motility (*3*−*5*), and endocytosis (*6*) among others. ADF/cofilin is an indispensable and ubiquitous protein in eukaryotes (*7*−*14*). Cofilin binds to both F-actin and G-actin and with a higher affinity to the ADP-bound state. ADF/Cofilin exerts two complementary activities: it severs actin filaments and enhances their turnover (*4*, *15*, *16*) by producing new filament ends that are available for polymerization/depolymerization (*16*−*18*). ADF/Cofilin activity is pH dependent, with the overall depolymerizing function being more efficient at alkaline pH (above 7.5) (*8*).

Several electron microscopy (*19*) and solution studies (*20*, *21*) suggested that the filament severing and depolymerizing activities of ADF/cofilin are linked to the overall weakening of longitudinal and lateral interprotomer contacts in F-actin by cofilin. However, understanding the mechanism of those events requires detailed information on the actin−ADF/cofilin binding contacts and their dynamic rearragements. In the absence of a 3-D structure of the complex, different approaches have been used to map binding surfaces between the two proteins. The structural homology between ADF/cofilin and gelsolin segment 1 (*22*, *23*) suggested that ADF/cofilin binds G-actin in a similar fashion. In another study, by Yonezawa et al. (*24*), cofilin was chemically cross-linked to the N-terminal portion (amino acids 1−12) of G-actin. The portion of cofilin that was cross-linked to actin was identified as equivalent to Arg^{96} and Lys^{98} in yeast cofilin. A synthetic dodecapeptide including the cofilin cross-linked amino acids, and corresponding to the sequence of Trp^{88}-Met^{99}, inhibited the binding of cofilin to G-actin, but this result was questioned as possibly reflecting nonspecific

† This work was supported by grants from USPHS to E.R. (GM-077190), to E.H.E. (AR042023), and to S.C.A. (GM53807); from the NSF to E.R. (MCB0316269); and from the U.S. Department of Energy to J.A.L. (DE-FC03-87ER60615).

* Corresponding author. Telephone: (310) 825-2668. Fax: (310) 206-7286. E-mail: reisler@mbi.ucla.edu.

‡ Department of Chemistry and Biochemistry, University of California, Los Angeles.

§ Department of Biological Chemistry, University of California, Los Angeles, CA.

$ Molecular Biology Institute, University of California, Los Angeles.

|| Hebrew University of Jerusalem, Israel.

⊥ Albert Einstein College of Medicine.

◊ University of Virginia.

Present address: Institute of Biochemistry, Cologne, Germany.

[1] Abbreviations: DNase I, deoxyribonuclease I; F-actin, filamentous actin; G-actin, monomer actin; S1, myosin subfragment 1; Tm, tropomyosin; WT, wild type; LC−MS/MS, liquid chromatography−tandem mass spectrometry; ADF, actin-depolymerization factor; AC, actin−cofilin dimer; FPLC, fast-performance liquid chromatography; MALDI−MS/MS, matrix-assisted laser desorption ionization−tandem mass spectrometry; SDS-PAGE, sodium dodecyl sulfate-polyacrylamide gel electrophoresis; PC, phenylcarbamyl; TFA, trifluoroacetic acid; PTC, phenylthiocarbamyl.

10.1021/bi0610754 CCC: $37.00
Published on Web 12/10/2006

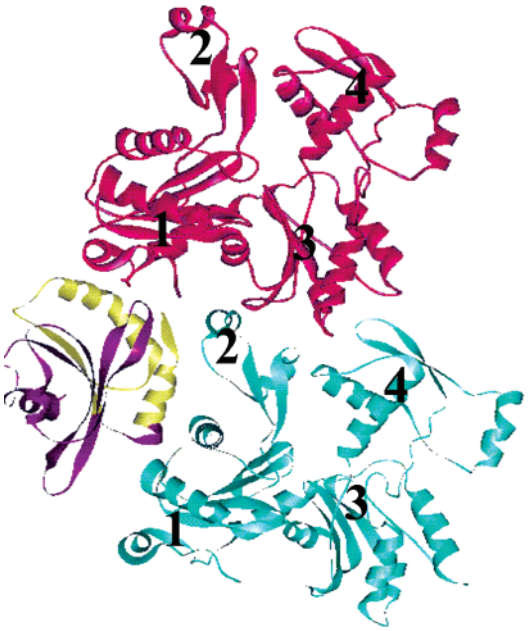

FIGURE 1: Schematic representation of cofilin−F-actin binding. Crystal structure of yeast cofilin is positioned along two adjacent protomers in the long pitch helix of the Holmes (*59*) model of the F-actin structure in a manner consistent with mutagenesis and cross-linking studies. The G-actin binding surface of cofilin (peptides colored in yellow) is identified on the basis of synchrotron protein footprinting analysis (*31*).

electrostatic interactions between the peptide and the actin (*25*). Systematic mutagenesis of yeast cofilin (*25*) did not confirm the assumption that gelsolin segment 1 and cofilin shared the same binding site, because of poor sequence conservation at the putative G-actin binding site.

In contrast, the same authors (*25*) concluded that the N terminus of cofilin, a portion of helix α3, and the turn connecting strand β6 and helix α4 were crucial for G-actin interaction. Others studies (*26*), including observations that the activity of ADF/cofilin is regulated by reversible phosphorylation of a serine residue in the N-terminal region (*27*−*30*), also support the importance of this site to actin binding. In a more recent study, Guan et al. (*31*) used synchrotron protein foot printing and implicated cofilin peptides 4−20, 10−17, 83−96, 91−105, and 106−117 in direct or indirect interactions with G-actin, consistent with previous biochemical and mutagenesis studies.

The residues on G- and F-actin that bind to cofilin are less well documented. Electron microscopy and image reconstruction studies (*32*) revealed that cofilin is intercalated between two actin protomers along the filament (at the cleft between subdomains 1 and 3 of the upper protomer and at subdomain 2 of the lower protomer). Figure 1 shows a schematic representation of the cofilin binding surface identified by footprinting (yellow) and the actin binding surface based on the cryomicroscopy work by McGough et al. (*32*). According to these authors, cofilin overlaps in the filament with the subdomain 2 region. This raises the question of whether a cofilin binding site(s) exists in the subdomain 2 region, perhaps too weak to be easily detected with G-actin but which may contribute to the binding of cofilin that already interacts with the subdomain 1/3 region on the adjacent protomer in F-actin.

The aim of this study was to probe for possible interaction of yeast cofilin with subdomain 2 of G-actin. We used cross-linking by transglutaminase as an approach for probing putative weak protein−protein interactions. This procedure involved cross-linking of Gln^{41} on skeletal α-actin to yeast cofilin, enzymatic digestion of the cross-linked proteins, and identification of the resulting cross-linked peptides by liquid chromatography−tandem mass spectrometry (LC−MS/MS) and matrix-assisted laser desorption/ionization−tandem mass spectrometry (MALDI−MS/MS). The identified actin−cofilin contact and EM analysis of filaments prepared from the cross-linked complex shed new light on how cofilin severs actin filaments.

MATERIALS AND METHODS

Reagents. Phenylisothiocyanate was obtained from Pierce (Rockford, IL); phenyl isocyanate, trimethylamine, and *n*-heptane were purchased from Acros Organics (Morris Plains, NJ). Pyrene maleimide was obtained from Molecular Probes (Eugene, OR), and all the other reagents were aquired from Sigma Chemical Co (St. Louis, MO).

Proteins. DNase I was purchased from Worthington Biochemical (Lakewood, NJ). Bacterial transglutaminase was provided generously by Dr. K. Seguro (Ajinomoto Co., Kawasaki, Japan). Sequencing grade modified trypsin and endoproteinase Lys-C were purchased from Promega Corporation (Madison, WI) and Wako Chemicals (Richmond, VA), respectively.

Skeletal actin was extracted from rabbit muscle acetone powder according to Spudich and Watt (*33*) and stored in G-buffer (5.0 mM Tris−HCl (pH 8.0), 0.2 mM $CaCl_2$, 0.2 mM ATP, 0.5 mM β-mercaptoethanol). The preparation of actin mutant Q41C was described earlier (*34*). Yeast actin was purified from yeast cells by affinity chromatography on a DNase I column (*35*). Cofilin expressed in *E. coli* was purified using a standard protocol (*20*). The concentrations of cofilin, actin, and DNase I were determined spectrophotometrically, using the extinction coefficients $\epsilon_{280}^{1\%} = 9.2$ cm^{-1}, $\epsilon_{290}^{1\%} = 11.5$ cm^{-1}, and $\epsilon_{280}^{1\%} = 11.1$ cm^{-1}, respectively. The concentration of yeast actin was measured by the Bradford protein assay (*36*).

Actin Labeling. The actin−cofilin cross-linked complex, FPLC-purified and free of DTT, was labeled with pyrene maleimide at 1.5 M reagent excess for 90 min at room temperature. The labeling was stopped with 1.0 mM DTT, and the excess reagent was removed by dialysis. The extent of labeling was 80%.

Transglutaminase Cross-Linking. Ca−G (skeletal)-actin (or Ca−G (yeast)-actin) saturated with yeast cofilin (1:2 mol ratio) was incubated with bacterial transglutaminase (0.2 unit/mL) in G-buffer for 1 h at room temperature. The reaction products were analyzed by sodium dodecyl sulfate-polyacrylamide gel electrophoresis (SDS-PAGE). The cross-linked complex was purified for subsequent experiments by fast-performance liquid chromatography (FPLC). The reaction mixture was loaded onto a Superdex-200 column (Amersham Pharmacia Biotech, Piscataway, NJ) equilibrated with G-buffer and operated at a flow rate of 1.0 mL/min. Fractions containing the cross-linked actin−cofilin complex were pooled and concentrated in the G-buffer.

Mass Spectrometry. After enzymatic proteolysis, online peptide sequencing was accomplished by liquid chromatography−tandem mass spectrometry (LC−MS/MS) on a quad-

rupole time-of-flight Applied Biosystems (Foster City, CA) QSTAR XL (QqTOF) mass spectrometer. The nano-LC was equipped with an LC Packings PepMap C18 precolumn (300 μm × 5 mm) and an LC Packings PepMap C18 column (75μm × 150 mm). The eluents used for the LC were (A) 5% ACN/water containing 0.1% FA and 0.01% TFA and (B) 95% ACN/water acid containing 0.1% FA and 0.01% TFA. The flow was 200 nL/min, and the following gradient was used: 5% B to 35% B in 15 min then 35% B to 80% B in 4 min and maintained at 80% B for 9 min. The column was reequilibrated with 5% B for 14 min before the next run. For online MS and MS/MS analyses, a New Objective (Woburn, MA) Pico Tip (id. 8 μm) was used for spraying with the voltage set at 2 kV. Protein identification was based on standard Mascot (Matrix Science, London, UK) criteria for statistical analysis of the LC−MS/MS data. For MALDI−MS/MS, α-cyano-4-hydroxy cinnamic acid or 2,5-dihydroxybenzoic acid was used as matrix. The protein mixture was diluted (1:50) in 20% *n*-propanol or 0.1% octyl glucoside for larger masses. The MS/MS fragmentation spectrum of cross-linked peptides was analyzed using the MS2Assign Automatic Structure Assignment Program (ASAP) (*37*).

HPLC Purification of Cofilin N-Terminal Peptide. Cofilin (500 μg) was reduced with 10 mM DTT (60 °C for 45 min), followed by alkylation with 24 mM iodoacetamide in darkness at 45 °C for 1 h. DTT (24 mM) was then added to quench the alkylation reaction. Cofilin was digested with Lys-C at a 1:50 enzyme/substrate ratio in 300 mM Tris−HCl (pH 8.0) at 37 °C for 24 h. The resulting peptides were separated on an Agilent ZORBAX 300SB C_{18} column (2.1 mm × 150 mm).

Peptide Ladder Sequencing. The 2037 Da peptide generated from Lys-C digestion of cofilin (2 nmol) was isolated by HPLC with fraction collection. The appropriate fraction was identified using matrix-assisted laser desorption/ionization (MALDI) on an Applied Biosystems (Farmingham, MA) Voyager DE-STR time-of-flight mass spectrometer operated in positive ion reflectron mode. To confirm the first three residues as Gly-Ser-Arg, the lyophilized peptide was then ladder sequenced (a variant of Edman degradation) (*38*). Peptide ladder sequencing consisted of two steps, as shown in Supporting Information. After two cycles, the mass spectra of cleavage products were recorded by MALDI−MS. The sequence was obtained by calculating mass differences between two adjacent peaks (Supporting Information).

Analytical Ultracentrifugation. Sedimentation velocity and sedimentation equilibrium runs were performed in a Beckman Optima XL-A analytical ultracentrifuge using 12 mm path length double sector cells and absorption optics. Sedimentation velocity was performed at speeds of 55 000 or 60 000 rpm at 20 °C. Sedimentation equilibrium was performed at speeds of 9000 and 11 000 rpm at 4 °C. Samples were examined at wavelengths of 290 nm for unlabeled proteins and at 342 nm for samples using pyrene-labeled actin. The protein concentration was 10−12.5 μM for the cross-linked actin−cofilin heterodimer or pyrene (actin)-labeled cross-linked actin−cofilin heterodimer and 10−37.5 μM for cofilin. All samples were in G-buffer. For sedimentation velocity runs, the sedimentation coefficient distribution was determined from a g(s*) versus s* plot using the Beckman Origin-based software (Version 3.01). This is a corrected plot of d*c*/d*t* (where *c* is the protein concentration) on the *y*-axis and apparent sedimentation coefficient on the *x*-axis, such that the *y*-axis gives the amount of material at the sedimentation coefficient indicated on the *x*-axis.

The predicted (theoretical) sedimentation coefficient for the actin−cofilin complex was calculated on the basis of the following considerations. The sedimentation coefficient for a protein is given by $S = M^{2/3}(1 - \bar{v}\rho)/N6\pi\eta(3\bar{v}/4\pi N)^{1/3}(f/f_o)$ (*39*, *40*), where M is the molecular weight of the protein, $\bar{v}$ is the partial specific volume of the protein, ρ is the density of the solvent, η is the viscosity of the solvent, and (f/f_o) is the ratio of the translational frictional coefficient to the translational frictional coefficient of a hydrodynamicly equivalent anhydrous sphere (this term includes the shape and hydration terms for the protein). We may thus write two equations, one for actin (a) and one for the actin−cofilin complex (ac). Dividing one by the other we get $S_{ac}/S_a = (M_{ac}/M_a)^{2/3}((1 - \bar{v}_{ac}\rho)/(1 - \bar{v}_a\rho)(\bar{v}_a/\bar{v}_{ac})^{1/3}(f/f_o)_a/(f/f_o)_{ac})$. As the partial specific volumes of actin (0.734 at 20 °C) and cofilin (0.731 at 20 °C) are similar, the second two terms are negligible (to within 1% error). The equation thus simplifies to $S_{ac}/S_a = (M_{ac}/M_a)^{2/3}(f/f_o)_a/(f/f_o)_{ac}$. To a first approximation, assuming $(f/f_o)_a = (f/f_o)_{ac}$, we obtain the $S_{ac}/S_a = (M_{ac}/M_a)^{2/3}$. The molecular weight of the bacterially expressed cofilin used here is 15 826 and that for actin is 41 874.

Sedimentation equilibrium runs were analyzed initially with a nonlinear least-squares exponential fit for a single ideal species to give a weight average molecular weight of all species in solution and then with a two-exponential fit, assuming two species in solution. Partial specific volumes (mL/g) of 0.734 (20 °C) and 0.727 (4 °C) for actin and 0.731 (20 °C) and 0.724 (4 °C) for cofilin were calculated using the amino acid composition and a temperature correction (*41*, *42*).

Electron Microscopy. Samples were mounted and negatively stained on electron microscope grids as previously described (*43*). Prior to EM observations, the actin−cofilin purified heterodimer complex was polymerized with 2.0 mM $MgCl_2$. Grids were examined in a Tecnai-12 electron microscope (Philips, The Netherlands) under minimal-dose conditions at an accelerating voltage of 80 keV and a nominal magnification of 30000×. Negatives were quantified with a Leaf 45 densitometer scanner, using a raster of 3.9 Å/pixel.

Electron Microscopy Image Analysis. The SPIDER software package (*44*) was used for image processing. From images of the polymerized cross-linked heterodimer complex of actin−cofilin, 6330 segments (each 100 pixels long, or ∼392 Å) were extracted. The overall reconstruction using the IHRSR method (*45*) revealed a symmetry of 159.4° rotation per subunit. To sort images into classes, four model volumes were used: regular F-actin (*46*), T1-actin (*47*), T2-actin (*47*), and cofilin-decorated F-actin (*48*). Helical twists of 150−170° per subunit, with a step size of 4°, were applied to each of these references, and the resultant volumes were rotationally projected with an increment of 4° to produce 2160 reference images (4 × 6 × 90). Raw images were cross-correlated with the references, and segments that possessed the best correlation with the cofilin-decorated F-actin having a twist of 162° ($n = 727$) were reconstructed.

A set of 9288 segments extracted from rabbit F-actin decorated with yeast cofilin was used as a control for decoration in the absence of cross-linking. The overall reconstruction of this set yielded a symmetry of 162.6°. The

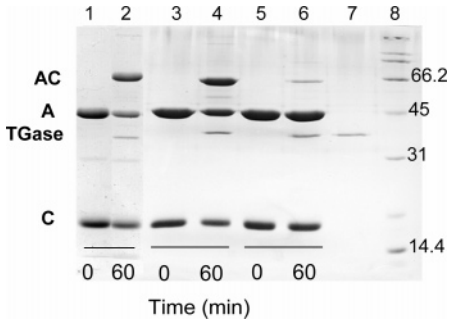

FIGURE 2: Cross-linking of cofilin to Ca−G-actin by transglutaminase. The formation of the Ca−G-actin (10 μM)−yeast cofilin (20 μM) cross-linked product was analyzed by 11% SDS-PAGE. Reaction aliquots were examined at different time points. A pattern of cross-linking yeast cofilin to rabbit skeletal actin (lanes 1 and 2), yeast WT actin (lanes 3 and 4), and yeast actin Q41C mutant (lanes 5 and 6) is shown only for 0 and 60 min reaction times. Tranglutaminase (lane 7) and molecular weight markers and their corresponding masses (lane 8) are also shown. The symbols A, C, TGase, and AC correspond to actin, cofilin, transglutaminase, and actin-cofilin heterodimer, respectively.

same sorting procedure was used to separate images into classes based upon occupancy and structural states of F-actin. A class of segments that possessed the best correlation with cofilin-decorated F-actin having a twist of 162° (n = 4,840) was used for reconstruction and converged to a symmetry of 162.3°. For both the cross-linked and control actin filaments, the error in determination of the twist was estimated by running the IHRSR procedure from three different starting points.

RESULTS

Cross-Linking of Actin to Cofilin and the Mapping of Cross-Linked Sites. Earlier work showed that Gln^{41} on G-actin has the highest reactivity toward transglutaminase and that it can be coupled readily to Lys^{50} on the DNase I binding loop with this enzyme (*49*). We used a similar protocol (*49*) to cross-link actin to cofilin. A mixture of yeast cofilin and rabbit skeletal Ca−G-actin (mol ratio 1:2 of actin/cofilin) was reacted with bacterial transglutaminase, and the products were examined by SDS-PAGE. The reaction results in the appearance of a single new band, corresponding to the molecular weight of 1:1 actin and cofilin complex (Figure 2). As estimated by SDS-PAGE stain intensities, between 50 and 85% of the G-actin can be cross-linked to cofilin in this way. The efficiency of this reaction is likely limited by the competing intramolecular cross-linking of Gln^{41} to Lys^{50} on G-actin. To confirm that the cross-linking indeed involves subdomain 2 of actin, we carried out two experiments. First, we confirmed that DNase I, which binds with high affinity to subdomain 2 (*50*), completely abolished the cross-linking of cofilin to G-actin (data not shown). In a second experiment, we compared transglutaminase reactions of cofilin with WT actin and the QC yeast actin mutant (in which Gln^{41} was replaced with cysteine). Although WT yeast actin was cross-linked to cofilin to the same extent as skeletal α-actin, only marginal cross-linking was achieved with the QC mutant (Figure 2). This shows that similar transglutaminase-mediated cross-linking occurs also in a homologous yeast actin/yeast cofilin system. Moreover, this result confirms that the main cross-linking of cofilin to actin involves Gln^{41} on actin and indicates the presence of a secondary cross-linking site on actin. Because the transglutaminase-mediated reaction depends primarily on the reactivity of the glutamine residue toward this enzyme, the fact that cofilin cross-linking to this second site is only marginal (in QC yeast actin) does not indicate its smaller importance to cofilin binding to G-actin.

Table 1: Transglutaminase Cross-Linked Tryptic and Lys-C Peptides from Actin−Cofilin

peptides	protease	cross-linked amino acids	cross-linked (MH^+) monoisotopic theoretical	cross-linked (MH^+) monoisotopic observed
Gly^1-Lys^{20} (cofilin)/ Ala^{19}-Lys^{50} (actin)	LysC	Gly^1 Gln^{41}	5327.70	5327.91
Gly^1-Arg^3 (cofilin)/ His^{40}-Lys^{50} (actin)	trypsin	Gly^1 Gln^{41}	1472.73	1472.71
Ser^{97}-Lys^{105} (cofilin)/ Gln^{360}-Phe^{375} (actin)	trypsin	Lys^{98} Gln^{360}	2919.40	2919.50

Mass Spectrometric Identification of Transglutaminase Cross-Linked Residues. We used LC−MS/MS analysis to map the cross-linking sites. The cross-linked actin−cofilin complex was purified by size exclusion chromatography, reduced, alkylated, and then digested with endoproteinase Lys-C in 6 M urea. Online HPLC−ESI−MS (ESI, electrospray ionization) of the actin−cofilin cleavage products revealed a unique peptide with a monoisotopic mass $[M + H]^+$ of 5327.9 Da in the digested, cross-linked preparation that was absent in an uncross-linked preparation (Table 1). This is consistent with a cross-link between the N-terminal peptide of recombinant cofilin (amino acids 1−20, theoretical monoisotopic mass 2036.0 Da) and the Gln^{41}-containing actin peptide 40−50 (amino acids 19−50, theoretical monoisotopic mass 3307.6 Da).

An aliquot of the Lys-C digest was digested further with trypsin to obtain smaller peptides more amenable to MS/MS. A unique peptide of mass $[M + H]^+$of 1472.7 Da was identified, and the product ion spectrum of the triply charged peptide was obtained (Figure 3). The product ions arising from peptide backbone cleavages allowed almost complete sequencing of the actin peptide and unequivocal assignment of Gln^{41} as the cofilin-linked residue.

The identification of the cross-linked residue on the N terminus of cofilin was more complicated. The N terminus does not contain a lysine, which could provide an ϵ-amino group from the side chain for the reaction. The N terminus could be the amino group donor but is reported as blocked in the WT protein. The N-terminal peptide mass that we measured was high by 57 Da, assuming initiator methionine excision. To check possible cross-linking targets, the N-terminal peptide of cofilin was purified by HPLC and subjected to ladder sequencing, according to a protocol adapted from B. Chait et al. (*38*) (Material and Methods). After two cycles of manually performed ladder-generating chemistry, a MALDI−TOF-MS spectrum of the mixture **(**Supporting Information**)** showed two peaks at m/z 2274.9 and 2217.9 differing by 57 Da, the mass of a glycine residue. The difference between the two following peaks in the ladder sequencing (2217.9 and 2130.9) is 87, corresponding to serine. Thus the amino terminus was non-acetylated glycine, revealing that Gly^1 participated in cross-linking to Gln^{41} on actin. This recombinant cofilin sequence was verified by sequencing of the cofilin plasmid DNA.

The MALDI mass spectrum of the trypsinized cross-linked actin cofilin revealed the presence of a secondary cross-linked

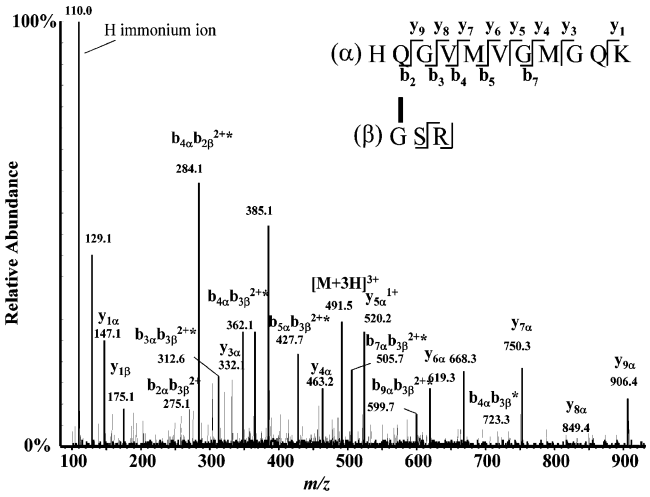

FIGURE 3: MS sequencing of the transglutaminase cross-linked actin−cofilin peptides. (A) MS/MS spectrum of the $[M + 3H]^{3+}$ of the transglutaminase cross-linked tryptic peptides at *m*/*z* 491.5. Peptide (α) is G-actin and peptide (*β*) is from yeast cofilin. Singly- and doubly-charged *y*-type product ions were generated from dissociation of the 3^+-charged precursor ion. (Peptide fragments were denoted following the nomenclature for fragmentation of cross-linked oligopeptides (*60*−*62*). Subscripts are used to denote the residue position, counting from the N terminus for a_n, b_n, and c_n ions and from the C terminus for x_n, y_n, and z_n products. A superscript is added to indicate the product ion charge state. Lack of a superscript denotes a singly charged fragment ion). The asterisk refers to a +18 Da product.

Table 2: MS Sequencing of the Transglutaminase Cross-Linked Actin−Cofilin Peptides

(*m*/*z*) theoretical	(*m*/*z*) observed	ion[a]	sequence tag
341.23	341.20	KMV (−18)	KMV
392.2	392.21	$y_{4\beta}$	ASSK
456.28	456.23	$[b_{2\alpha}\, b_{2\beta}]^+$	QE-SK
619.42	619.29	$[b_{3\alpha}\, b_{2\beta}]^+$	QEY-SK
750.37	750.33	$b_{7\beta}(-17)$	KMVYASS (−17)
768.40	768.36	$y_{7\beta}(-17)$	MVYASSK
785.38	785.38	$y_{7\beta}$	MVYASSK
846.47	846.44	$y_{6\alpha}$	VHRKCF
949.63	949.39	$a_{9\alpha}$	QEYDEAGPS
960.61	960.35	$b_{9\alpha}(-17)$	QEYDEAGPS
1024.54	1024.54	$[b_{1\alpha}\, y_{8\beta}]^+$	Q-KMVYASSK
1153.78	1153.58	$[b_{2\alpha}\, y_{8\beta}]^+$	QE-KMVYASSK
1200.77	1200.63	$y_{10\alpha}$	GPSIVHRKCF
1414.60	1414.61	$[b_{5\alpha}\, b_{7\beta}]^+$	QEYDE-SKMVYAS
1560.70	1560.71	$[b_{8\beta}\, y_{5\alpha}]^+$	QEYDE-KMVYASSK

[a] MS/MS ions of the $[M + H]^+$ of the transglutaminase cross-linked tryptic peptides at *m*/*z* 2919.50. Peptide (α) is G-actin, and peptide *β* is from yeast cofilin.

site. The existence of a secondary cross-linking site on actin was confirmed by observing this reaction, which occurred to a minor extent with cofilin and the QC yeast actin mutant (Figure 2). Theoretical and experimental masses of the tryptic peptides with their corresponding cross-links are listed in Table 1. The observed $[M + H]^+$ ion of *m*/*z* 2919.50 was further sequenced by MALDI−MS/MS and the corresponding tandem mass spectra results are presented in Table 2. The MS/MS data support a cross-link between Gln^{360} in actin and Lys^{98} on cofilin.

Analytical Ultracentrifugation. Analytical ultracentrifugation was used to characterize the FPLC-purified actin−cofilin heterodimer and its interaction with cofilin at concentrations (10 μM or greater) far above the K_d of actin for cofilin, 0.05 μM (*20*).

Assuming no large shape change in actin upon the formation of the actin−cofilin heterodimer (or heterotrimer), the ratio of sedimentation coefficients of the complex and G-actin should be proportional to the two-thirds power of the ratio of their molecular weights (M_w) (Materials and Methods). Because the sedimentation coefficient of G-actin (in G-actin buffer) was 3.25 S (data not shown), we may calculate the sedimentation coefficient of the actin−cofilin heterodimer as $S = 3.25(M_{w,actin-cofilin}/M_{w,actin})^{2/3} = 4.03$ S. If this heterodimer were to bind an additional cofilin, the predicted sedimentation coefficient would be 4.74 S (For comparison, the predicted sedimentation coefficient for a dimer of the actin−cofilin heterodimer (i.e., $actin_2$−$cofilin_2$) is 6.4 S).

The actin−cofilin heterodimer (10 μM) sedimented as a somewhat heterogeneous small aggregate with a sedimentation coefficient of 10.0−11.4 S, depending on the preparation (Figure 4A). In the presence of additional (10 μM) cofilin, a heterogeneous peak with an approximate sedimentation coefficient of 6.2−6.7 S was observed, indicating that additional cofilin was breaking up the aggregates. When the cofilin concentration was raised to 20 μM, giving a cofilin/actin−cofilin heterodimer ratio of 2:1, a slow peak (sedimentation coefficient $\sim$ 1.5 S), corresponding to unbound cofilin, and a relatively homogeneous peak of 4.6−4.8 S, corresponding to actin-$cofilin_2$, were observed. To observe this peak free of spectroscopic interference from the excess cofilin, an actin−cofilin heterodimer labeled with pyrene on the actin was prepared. When cofilin (25 μM) was added to the pyrene-labeled actin−cofilin heterodimer (12.5 μM) and the solution was observed at 342 nm (so that only complexes containing actin could be seen), a major symmetrical peak with a sedimentation coefficient of 4.75 S, corresponding to actin−$cofilin_2$, and a small amount of higher aggregate were observed (Figure 4B).

Sedimentation equilibrium experiments yield the weight-average molecular weight of all complexes observed in solution, independent of the shape assumption used above. Thus, to confirm the results of sedimentation velocity experiments, we performed sedimentation equilibrium measurements on the pyrene-labeled actin−cofilin heterodimer (12.5 μM) in the presence of excess cofilin (25 μM). As above, we monitored the absorbance at 342 nm so that only the molecular weight of actin-containing complexes was determined. The molecular weights so determined were 82 200 at 9000 rpm and 81 500 at 11 000 rpm, consistent with the major species in solution being actin−$cofilin_2$ but somewhat higher than the predicted molecular weight for actin−$cofilin_2$, 73 500. The speed dependence of the molecular weight and nonrandom nature of the residuals to the fit suggested this was due to a small amount of aggregate (seen in the sedimentation velocity runs). Alternatively, the observed molecular weights might be due to a major actin−$cofilin_3$ complex and an unknown lower molecular weight contaminant. This latter possibility could be ruled out because fitting individual data scans to a double-exponential expression with the molecular weight of one component fixed at that of actin−$cofilin_3$, and the concentration of both components and the molecular weight of the second component allowed to float, yielded absurd results (negative molecular

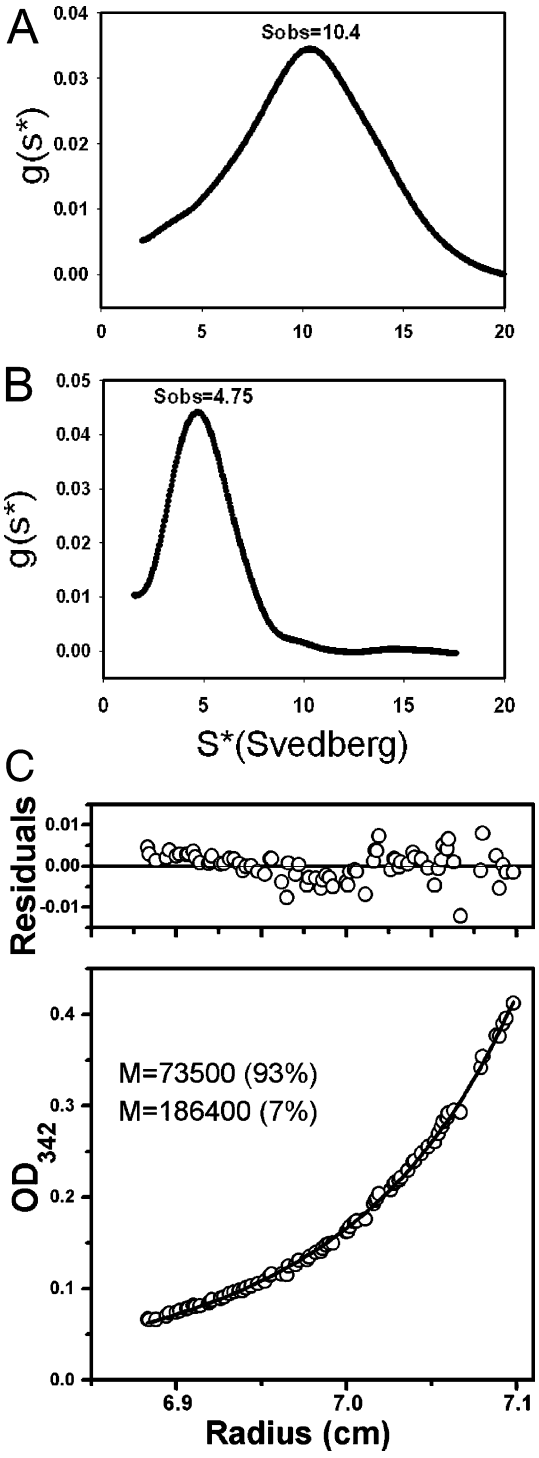

FIGURE 4: Analytical ultracentrifugation of the cross-linked actin−cofilin heterodimer in the absence and presence of cofilin. (A) Sedimentation coefficient distribution of the cross-linked actin−cofilin heterodimer (10 μM); protein concentration was monitored by absorbance at 290 nm. (B) Sedimentation coefficient distribution of the pyrene (actin)-labeled cross-linked actin−cofilin heterodimer (12.5 μM) in the presence of cofilin (12.5 μM), as monitored by pyrene absorbance at 342 nm. Both runs were performed at 55 000 rpm and 20 °C. (C) Sedimentation equilibrium. A double-exponential fit (solid line) to data (circles) collected at 4 °C at a rotor speed of 11 000 rpm, with absorbance measured at $\lambda = 342$ nm for a mixture of 12.5 μM actin−cofilin heterodimer (pyrene-labeled actin) and 25 μM cofilin. Residual errors are presented in the upper panel. The gap in data between 7.067 and 7.079 cm is an artifact of the data collection system.

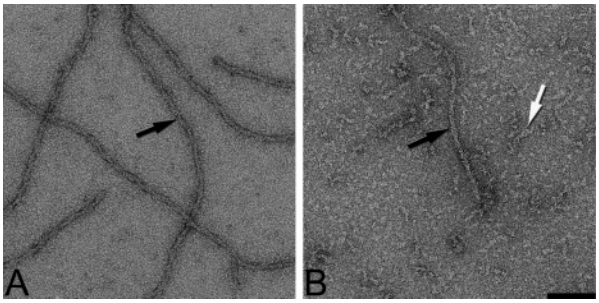

FIGURE 5: Electron micrographs of control skeletal F-actin decorated with yeast cofilin (A) and a product of polymerization of cross-linked heterodimer complex of actin−cofilin (B). In the presence of excess of yeast cofilin, actin filaments are long and uniformly decorated (A, black arrow). Cross-linked actin−cofilin is present as a mixture of aggregates (white arrow) and short filaments (B, black arrow). The bar represents 500 Å.

weights for the second component). However, when similar fits were performed using the molecular weight of actin−cofilin$_2$, the data could be fit well by a mixture containing, depending on the scan, 87−93% actin−cofilin$_2$ and 13−7% larger aggregate (Figure 4C). The molecular weight of the larger component, which is present in small amounts, was poorly constrained, varying from about 180 000 to 270 000. Because the fundamental covalent unit here is the cross-linked actin−cofilin, which as shown by sedimentation velocity forms small aggregates that are broken up by addition of cofilin, it is likely that this higher molecular weight material represents some residual actin−cofilin aggregates, consisting of (actin−cofilin)$_n$, where n is approximately 3−5.

Electron Microscopy. Addition of 2.0 mM $MgCl_2$ to the solution of cross-linked AC resulted in a major transformation of the 10−11 S oligomers into mostly short actin filaments containing the cross-linked cofilin (Figure 5B). Although rabbit F-actin filaments decorated with yeast cofilin are long and uniform (Figure 5A), much of the polymerized cross-linked heterodimer complex is found in aggregates (Figure 5B, white arrow). However, both the cross-linked and uncross-linked filaments have the same diameter. We did not find any substantial fraction of naked segments in the control filaments; ~60% of the heterodimer filaments were found to have cross-linked cofilin disordered and not visible in our electron density maps (data not shown). Interestingly, the mean twist found for the control filaments decorated with cofilin was 162.62 ± 0.01° (SEM), and the heterodimer filaments had a mean twist of 159.4 ± 0.8° (SEM). The significant difference in twist suggests that the cross-link introduced some small structural perturbation into the interaction of cofilin with F-actin. Because only ~40% of segments have cross-linked cofilin visualized as tightly bound to F-actin, the fact that these short filament are significantly twisted is evidence of the cooperative propagation of twist along the actin filament. Despite this small difference, the 3-D reconstructions of the cross- and un-cross-linked cofilin−actin filaments are nearly indistinguishable (Figure 6), showing that the cross-link does not change the overall mode of binding of cofilin to F-actin.

DISCUSSION

Chemical cross-linking combined with MS and MS/MS analysis has emerged as an important approach for mapping

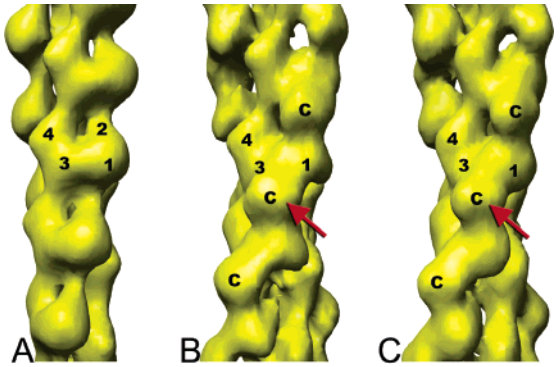

FIGURE 6: 3-D reconstruction of actin filaments. (A) Skeletal F-actin (*46*). (B) Skeletal F-actin decorated with yeast cofilin. (C) Segments of cross-linked actin−cofilin complex where cofilin is tightly bound. Actin subdomains are numbered in black, and the position of cofilin is indicated by "C". The position of cross-linked cofilin (C, red arrow in C) is indistinguishable from that in the filaments where cofilin has not been cross-linked to actin protomers (C, red arrow in B).

protein−protein interactions. The distances between the cross-linked sites obtained from such experiments provide constraints on the structure of the protein compexes. Also important to note is that cross-linking enables the detection and mapping of weakly bound protein complexes through a progressive accumulation of reaction products.

In the present study, we tested the premise that the likely interaction of cofilin with the subdomain 2 region in F-actin implies the presence of a weak or cryptic recognition site for cofilin in that structural element of G-actin in addition to the main cofilin binding site in the subdomain 1/3 region. We examined the possible secondary interaction between cofilin and subdomain 2 in G-actin by transglutaminase-mediated cross-linking, originating from Gln^{41} on the DNase I binding loop. Our cross-linking mapping reaveled that Gly^{1} in the recombinant cofilin's N terminus is positioned near Gln^{41} in subdomain 2 of G-actin, providing evidence for a transient and weak cofilin interaction with that subdomain. The complete blocking of such interaction by DNase I and the 1:1 stoichiometry of cofilin binding to G-actin (as determined in solution measurements (*14*)) demonstrated that the interaction detected by cross-linking between subdomain 2 and cofilin must be indeed weak.

The N-terminal region of cofilin, containing the regulatory phosphorylation site at Ser^{3}, and the helix α3 have been implicated in actin binding in several prior studies (*24*−*26*, *51*, *52*). Although cross-linking results do not impose sufficient constrains on prior models of actin−cofilin to allow for their refinement, we can suggest a possible orientation of cofilin within the actin−actin interface. Transplanted to the F-actin environment, our results suggest that Gly^{1} on cofilin is proximal to Gln^{41} in subdomain 2 of the lower protomer, and Lys^{98} on cofilin is in close proximity to Gln^{360} in subdomain 3 of the upper protomer. An earlier structural model for UNC-60B (*52*) suggested that the N terminus and the residues of the first half of the helix α3 (Val^{113}-Ser^{113} in UNC-60B, i.e., Val^{95}-Ser^{104} in yeast cofilin) would be positioned near the actin interface. This is consistent with the amino acids we found to be involved in actin binding, although the N terminus of UNC-60B is closer to subdomain 1 of the upper protomer than it is to subdomain 2 of the lower actin. We do not consider this difference to be significant because of the close proximity and mobility of the subdomain 2 and C-terminal regions on the adjacent actins (*43*, *53*). Our results agree also with the description by McGough et al. (*32*) of cofilin binding to F-actin on the basis of electron microscopy reconstruction studies. Their fitted cofilin makes contact with subdomain 2 of the lower protomer, and Gln^{41} is included in the list of residues within or near the cofilin binding site. Because the binding at subdomain 2 represents a weak or cryptic binding site for G-actin on cofilin, it is not related to or compared to prior models of strong cofilin binding to G-actin (*23*).

Solution Properties. The assumption that cross-linking of Gln^{41} to the cofilin N terminus captures an interaction that is amplified and important in F-actin prompted us to examine the solution properties and polymerization of the purified cross-linked AC complex. The fact that in G-buffer this complex forms heterogeneous oligomers (∼10.5 S) can be rationalized by the affinity of cofilin cross-linked to subdomain 2 of one actin to bind to its otherwise primary subdomain 1/3 target, which is in this case on another cross-linked AC heterodimer. A simple prediction from such a model of head-to-tail association of AC dimers, with cofilin bridging between two actin molecules, is that the oligomers should be dissociated with the addition of free cofilin, which would compete with the cross-linked cofilin for binding to the subdomain 1/3 sites on AC. The confirmation of this prediction in our sedimentation velocity and equilibrium experiments adds credence to the above explanation of the AC oligomerization in G-buffer.

Electron Microscopy. The first important result of the EM analysis of F-actin formed from the cross-linked AC is that the position of tightly bound cross-linked cofilin in these filaments is virtually indistinguishable from that observed in the uncross-linked actin decorated by cofilin. This result validates the assumption that cofilin cross-linking to G-actin most likely captures cofilin proximity and interactions that exist in F-actin, but only in a cryptic form in G-actin, and does not distort the distribution of dynamic filament states.

The second important result is that a considerable fraction of the cross-linked cofilin (∼60%) cannot be fitted into electron density maps of the filaments, suggesting that these cofilin molecules are disordered despite their tethering to Gln^{41}. Cofilin disordering, which already has been described in the uncross-linked F-actin−cofilin complexes (*48*), may be connected to the recently reported disordering of subdomain 2 in F-actin−cofilin (*54*) and may result from transient detachment of cofilin from one of its two interaction sites on two consecutive actin protomers in the filament. We propose that in the latter case, when cofilin is bound transiently to only one actin, it no longer provides a stabilizing "bridge" to the local filament structure, thereby facilitating its severing. Such a scenario could explain why filaments fully saturated by cofilin undergo severing despite the calorimetric evidence for their thermal stabilization (*55*, *56*). The dynamic events that lead to transient populations of cofilin bound to two- and one-actin protomers are pertinent to the rapid severing process but may be transparent to the time-averaged calorimetry assays. As suggested in our recent study, the filaments are probably severed preferentially at sites of accumulated torsional strain and unoccupied by cofilin, i.e., free of its partial stabilizing effect. In agreement with this, it has been shown that the predicted cofilin cluster

sizes on F-actin required for efficient severing are small (*57*) and that cofilin binding increases cooperatively the filament tortional flexibility, therefore propagating the signal to naked portions of the filament (*58*). This is consistent with our observation that the cross-linked cofilin introduces an even greater change of twist to a normal actin filament than uncross-linked cofilin. At the same time, the cofilin is visualized as bridging two adjacent protomers in only ~40% of the segments examined, even though the cofilin must be physically attached in all of these regions. It is under these conditions of a large change of twist and a "partial" occupancy of cofilin molecules bound in a regular and ordered manner that only short filaments are observed. This suggests that the cross-linking of the N terminus of cofilin to Gln^{41} of actin enhances depolymerization abilities of yeast cofilin.

ACKNOWLEDGMENT

We are grateful to Helty Adisetiyo for skillful assistance. UCLA Proteomics Center (used for the mapping of the cross-linked complexes) was established and equipped with a grant from the W. M. Keck Foundation.

SUPPORTING INFORMATION AVAILABLE

Two figures (S1 and S2) containing MALDI spectra of actin−cofilin peptides included in the Supporting Information. This material is available free of charge via the Internet at http://pubs.acs.org.

REFERENCES

1. Abe, H., Obinata, T., Minamide, L. S., and Bamburg, J. R. (1996) *Xenopus laevis* actin-depolymerizing factor/cofilin: a phosphorylation- regulated protein essential for development, *J. Cell Biol. 132*, 871−885.
2. Gunsalus, K. C., Bonaccorsi, S., Williams, E., Verni, F., Gatti, M., and Goldberg, M. L. (1995) Mutations in twinstar, a Drosophila gene encoding a cofilin/ADF homologue, result in defects in centrosome migration and cytokinesis, *J. Cell Biol. 131*, 1243−1259.
3. Aizawa, H., Sutoh, K., and Yahara, I. (1996) Overexpression of cofilin stimulates bundling of actin filaments, membrane ruffling, and cell movement in Dictyostelium, *J. Cell Biol. 132*, 335−344.
4. Carlier, M. F., Laurent, V., Santolini, J., Melki, R., Didry, D., Xia, G. X., Hong, Y., Chua, N. H., and Pantaloni, D. (1997) Actin Depolymerizing Factor (ADF/Cofilin) Enhances the Rate of Filament Turnover: Implication in Actin-based Motility, *J. Cell Biol. 136*, 1307−1322.
5. Rosenblatt, J., Agnew, B. J., Abe, H., Bamburg, J. R., and Mitchison, T. J. (1997) Xenopus Actin Depolymerizing Factor/Cofilin (XAC) Is Responsible for the Turnover of Actin Filaments in Listeria monocytogenes Tails, *J. Cell Biol. 136*, 1323−1332.
6. Lappalainen, P., and Drubin, D. G. (1997) Cofilin promotes rapid actin filament turnover in vivo, *Nature 388*, 78−82.
7. Abe, H., Endo, T., Yamamoto, K., and Obinata, T. (1990) Sequence of cDNAs Encoding Actin Depolymerizing Factor and Cofilin of Embryonic Chicken Skeletal Muscle: Two Functionally Distinct Actin-Regulatory Proteins Exhibit High Structural Homology, *Biochemistry 29*, 7420−7425.
8. Hawkins, M., Pope, B., Maciver, S. K., and Weeds, A. G. (1993) Human Actin Depolymerizing Factor Mediates a pH-Sensitive Destruction of Actin Filaments, *Biochemistry 32*, 9985−9993.
9. Iida, K., Moriyama, K., Matsumoto, S., Kawasaki, H., Nishida, E., and Yahara, I. (1993) Isolation of a yeast essential gene, COF1, that encodes a homologue of mammalian cofilin, a low-M(r) actin-binding and depolymerizing protein, *Gene* 124, 115−120.
10. Moon, A. L., Janmey, P. A., Louie, K. A., and Drubin, D. G. (1993) Cofilin is an essential component of the yeast cortical cytoskeleton, *J. Cell Biol. 120*, 421−435.
11. Nishida, E., Muneyuki, E., Maekawa, S., Ohta, Y., and Sakai, H. (1985) An Actin-Depolymerizing Protein (Destrin) from Porcine Kidney−Its Action on F-Actin Containing Or Lacking Tropomyosin, *Biochemistry 24*, 6624−6630.
12. Adams, M. E., Minamide, L. S., Duester, G., and Bamburg, J. R. (1990) Nucleotide Sequence and Expression of a cDNA Encoding Chick Brain Actin Depolymerizing Factor, *Biochemistry 29*, 7414−7420.
13. Moriyama, K., Matsumoto, S., Nishida, E., Sakai, H., and Yahara, I. (1990) Nucleotide-Sequence of Mouse Cofilin cDNA, *Nucleic Acids Res. 18*, 3053.
14. Nishida, E., Maekawa, S., and Sakai, H. (1984) Cofilin, A Protein in Porcine Brain That Binds to Actin-Filaments and Inhibits Their Interactions with Myosin and Tropomyosin, *Zool. Sci. 1*, 903.
15. Bamburg, J. R., McGough, A., and Ono, S. (1999) Putting a new twist on actin: ADF/cofilins modulate actin dynamics, *Trends Cell Biol. 9*, 364−370.
16. Ichetovkin, I., Han, J. H., Pang, K. M., Knecht, D. A., and Condeelis, J. S. (2000) Actin filaments are severed by both native and recombinant Dictyostelium cofilin but to different extents, *Cell Motil. Cytoskeleton 45*, 293−306.
17. Blanchoin, L., and Pollard, T. D. (1999) Mechanism of Interaction of Acanthamoeba Actophorin (ADF/Cofilin) with Actin Filaments, *J. Biol. Chem. 274*, 15538−15546.
18. Du, J., and Frieden, C. (1998) Kinetic Studies on the Effect of Yeast Cofilin on Yeast Actin Polymerization, *Biochemistry 37*, 13276−13284.
19. McGough, A., and Chiu, W. (1999) ADF/Cofilin weakens lateral contacts in the actin filament, *J. Mol. Biol. 291*, 513−519.
20. Bobkov, A. A., Muhlrad, A., Kokabi, K., Vorobiev, S., Almo, S. C., and Reisler, E. (2002) Structural Effects of Cofilin on Longitudinal Contacts in F-actin, *J. Mol. Biol. 323*, 739−750.
21. Bobkov, A. A., Muhlrad, A., Shvetsov, A., Benchaar, S., Scoville, D., Almo, S. C., and Reisler, E. (2004) Cofilin (ADF) Affects Lateral Contacts in F-actin, *J. Mol. Biol. 337*, 93−104.
22. Hatanaka, H., Ogura, K., Moriyama, K., Ichikawa, S., Yahara, I., and Inagaki, F. (1996) Tertiary Structure of Destrin and Structural Similarity between Two Actin-Regulating Protein Families, *Cell 85*, 1047−1055.
23. Wriggers, W., Tang, J. X., Azuma, T., Marks, P. W., and Janmey, P. A. (1998) Cofilin and gelsolin segment-1: molecular dynamics simulation and biochemical analysis predict a similar actin binding mode, *J. Mol. Biol. 282*, 921−932.
24. Yonezawa, N., Nishida, E., Iida, K., Kumagai, H., Yahara, I., and Sakai, H. (1991) Inhibition of actin polymerization by a synthetic dodecapeptide patterned on the sequence around the actin-binding site of cofilin, *J. Biol. Chem. 266*, 10485−10489.
25. Lappalainen, P., Fedorov, E. V., Fedorov, A. A., Almo, S. C., and Drubin, D. G. (1997) Essential functions and actin-binding surfaces of yeast cofilin revealed by systematic mutagenesis, *EMBO J. 16*, 5520−5530.
26. Sutoh, K., and Mabuchi, I. (1989) End-Label Fingerprintings Show That an N-Terminal Segment of Depactin Participates in Interaction with Actin, *Biochemistry 28*, 102−106.
27. Agnew, B. J., Minamide, L. S., and Bamburg, J. R. (1995) Reactivation of Phosphorylated Actin Depolymerizing Factor and Identification of the Regulatory Site, *J. Biol. Chem. 270*, 17582−17587.
28. Morgan, T. E., Lockerbie, R. O., Minamide, L. S., Browning, M. D., and Bamburg, J. R. (1993) Isolation and characterization of a regulated form of actin depolymerizing factor, *J. Cell Biol. 122*, 623−633.
29. Arber, S., Barbayannis, F. A., Hanser, H., Schneider, C., Stanyon, C. A., Bernard, O., and Caroni, P. (1998) Regulation of actin dynamics through phosphorylation of cofilin by LIM-kinase, *Nature 393*, 805−809.
30. Yang, N., Higuchi, O., Ohashi, K., Nagata, K., Wada, A., Kangawa, K., Nishida, E., and Mizuno, K. (1998) Cofilin phosphorylation by LIM-kinase 1 and its role in Rac-mediated actin reorganization, *Nature 393*, 809−812.
31. Guan, J. Q., Vorobiev, S., Almo, S. C., and Chance, M. R. (2002) Mapping the G-Actin Binding Surface of Cofilin Using Synchrotron Protein Footprinting, *Biochemistry 41*, 5765−5775.
32. McGough, A., Pope, B., Chiu, W., and Weeds, A. (1997) Cofilin Changes the Twist of F-Actin: Implications for Actin Filament Dynamics and Cellular Function, *J. Cell Biol. 138*, 771−781.
33. Spudich, J. A., and Watt, S. (1971) The regulation of rabbit skeletal muscle contraction. I. Biochemical studies of the interaction of

the tropomyosin complex with actin and the proteolytic fragments of myosin, *J. Biol. Chem.* 4866−4871.
34. Kim, E., Wriggers, W., Phillips, M., Kokabi, K., Rubenstein, P. A., and Reisler, E. (2000) Cross-linking constraints on F-actin structure 1, *J. Mol. Biol. 299*, 421−429.
35. Cook, R. K., Root, D., Miller, C., Reisler, E., and Rubenstein, P. A. (1993) Enhanced stimulation of myosin subfragment 1 ATPase activity by addition of negatively charged residues to the yeast actin NH2 terminus, *J. Biol. Chem. 268*, 2410−2415.
36. Bradford, M. M. (1976) A rapid and sensitive method for the quantitation of microgram quantities of protein utilizing the principle of protein-dye binding, *Anal. Biochem. 72*, 248−254.
37. Schilling, B., Row, R. H., Gibson, B. W., Guo, X., and Young, M. M. (2003) MS2Assign, automated assignment and nomenclature of tandem mass spectra of chemically crosslinked peptides, *J. Amer. Soc. Mass Spectrom. 14*, 834−850.
38. Chait, B. T., Wang, R., Beavis, R. C., and Kent, S. B. H. (1993) Protein ladder sequencing, *Science 262*, 89−92.
39. Svedberg, T. and Pedersen, K. O. (1940) *The Ultracentrifuge*, pp 35−40, Oxford University Press, Oxford, U.K.
40. Cantor, C. R., and Schimmel, P. R. (1980) *Biophysical Chemistry Part II Techniques for the Study of Biological Structure and Function*, pp 609−610, W. H. Freeman and Company, New York.
41. Laue, T. M., Shah, B. D., Ridgeway, T. M., and Pelletier, S. L. (1992) Computer-aided interpretation of analytical sedimentation data for proteins, in *Analytical Ultracentrifugation in Biochemistry and Polymer Science* (Harding, S. E., Rowe, A. J., and Horton, J. C., Eds.) pp 90−125, Royal Society of Chemistry, Cambridge, U.K.
42. Cohn, E. J., and Edsall, J. T (1943) Density and apparent specific Vol. of proteins, in *Proteins, Amino Acids, and Peptides as Ions and Dipolar Ions*, (Cohn, E. J., and Edsall, J. T., Eds.) pp 370−381, Rheinhold Publishing, New York..
43. Kim, E., Phillips, M., Hegyi, G., Muhlrad, A., and Reisler, E. (1998) Intrastrand Cross-Linked Actin between Gln-41 and Cys-374. II. Properties of Cross-Linked Oligomers, *Biochemistry 37*, 17793−17800.
44. Frank, J., Radermacher, M., Penczek, P., Zhu, J., Li, Y., Ladjadj, M., and Leith, A. (1996) SPIDER and WEB: Processing and Visualization of Images in 3D Electron Microscopy and Related Fields, *J. Struct. Biol. 116*, 190−199.
45. Egelman, E. H. (2000) A robust algorithm for the reconstruction of helical filaments using single-particle methods, *Ultramicroscopy 85*, 225−234.
46. Orlova, A., Galkin, V. E., VanLoock, M. S., Kim, E., Shvetsov, A., Reisler, E., and Egelman, E. H. (2001) Probing the structure of F-actin: cross-links constrain atomic models and modify actin dynamics, *J. Mol. Biol. 312*, 95−106.
47. Galkin, V. E., Orlova, A., Koleske, A. J., and Egelman, E. H. (2005) The Arg Non-receptor Tyrosine Kinase Modifies F-actin Structure, *J. Mol. Biol. 346*, 565−575.
48. Galkin, V. E., Orlova, A., Lukoyanova, N., Wriggers, W., and Egelman, E. H. (2001) Actin Depolymerizing Factor Stabilizes an Existing State of F-Actin and Can Change the Tilt of F-Actin Subunits, *J. Cell Biol. 153*, 75−86.
49. Eli-Berchoer, L., Hegyi, G., Patthy, A., Reisler, E., and Muhlrad, A. (2000) Effect of intramolecular cross-linking between glutamine-41 and lysine-50 on actin structure and function, *Muscle Res. Cell Motil. 21*, 405−414.
50. Pollard, T. D. (1990) Actin, *Curr. Opin. Cell Biol. 2*, 33−40.
51. Pope, B. J., Gonsior, S. M., Yeoh, S., McGough, A., and Weeds, A. G. (2000) Uncoupling actin filament fragmentation by cofilin from increased subunit turnover, *J. Mol. Biol. 298*, 649−661.
52. Ono, S., McGough, A., Pope, B. J., Tolbert, V. T., Bui, A., Pohl, J., Benian, G. M., Gernert, K. M., and Weeds, A. G. (2001) The C-terminal Tail of UNC-60B (Actin Depolymerizing Factor/Cofilin) Is Critical for Maintaining Its Stable Association with F-actin and Is Implicated in the Second Actin-binding Site, *J. Biol. Chem. 276*, 5952−5958.
53. Kim, E., and Reisler, E. (1996) Intermolecular coupling between loop 38−52 and the C-terminus in actin filaments, *Biophys. J. 71*, 1914−1919.
54. Galkin, V. E., Orlova, A., VanLoock, M. S., Shvetsov, A., Reisler, E., and Egelman, E. H. (2003) ADF/cofilin use an intrinsic mode of F-actin instability to disrupt actin filaments, *J. Cell Biol. 163*, 1057−1066.
55. Dedova, I. V., Nikolaeva, O. P., Mikhailova, V. V., dos Remedios, C. G., and Levitsky, D. I. (2004) Two opposite effects of cofilin on the thermal unfolding of F-actin: a differential scanning calorimetric study, *Biophys. Chem. 110*, 119−128.
56. Bobkov, A. A., Muhlrad, A., Pavlov, D. A., Kokabi, K., Yilmaz, A., and Reisler, E. (2006) Cooperative Effects of Cofilin (ADF) on Actin Structure Suggest Allosteric Mechanism of Cofilin Function, *J. Mol. Biol. 356*, 325−334.
57. De La Cruz, E. M. (2005) Cofilin Binding to Muscle and Non-muscle Actin Filaments: Isoform-dependent Cooperative Interactions, *J. Mol. Biol. 346*, 557−564.
58. Prochniewicz, E., Janson, N., Thomas, D. D., and De La Cruz, E. M. (2005) Cofilin Increases the Torsional Flexibility and Dynamics of Actin Filaments, *J. Mol. Biol. 353*, 990−1000.
59. Holmes, K. C., Popp, D., Gebhard, W., and Kabsch, W. (1990) Atomic model of the actin filament, *Nature 347*, 44−49.
60. Roepstorff, P., and Fohlman, J. (1984) Proposal for a Common Nomenclature for Sequence Ions in Mass-Spectra of Peptides, *Biomed. Mass Spectrom. 11*, 601.
61. Biemann, K. (1990) Nomenclature for peptide fragment ions (positive ions), *Methods Enzymol. 193*, 886−887.
62. Biemann, K. (1988) Contributions of mass spectrometry to peptide and protein structure, *Biol. Mass Spectrom. 16*, 99−111.

BI0610754